Exploration of Trimetallic Nanoparticles as Electrocatalysts for Oxygen Reduction

A. Ezeta-Mejía[*], *J.M. Mora-Hernández, J.M. Hallen-López, E.M. Arce-Estrada*

Instituto Politécnico Nacional. ESIQIE. Departamento de Ingeniería Metalúrgica, UPALM Ed. 7, 07738, México D.F., México.
[*]E-mail: araceli-ezeta@hotmail.com

Oxygen reduction nanometric trimetallic RuXMo (X=Se,Sn) electrocatalysts have been prepared by mechanical alloying. The nanostructured catalysts were characterized by X-ray diffraction and Scanning electron microscopy. Homogeneous catalysts particles supported on Vulcan carbon were investigated by rotating disk electrode for the oxygen reduction reaction (ORR) in 0.5 M H_2SO_4. Results reveal improved specific activities toward the ORR with multielectron transfer process (n=4e-) to water formation. The RuSnMo presented a slightly higher electrocatalytic activity than RuSeMo due to its structural characteristics.

1. INTRODUCTION

Proton exchange membrane fuel cell (PEMFC) represents an environmentally friendly technology to produce electricity by direct electrochemical conversion of hydrogen and oxygen into water. However, two factors that limit its commercialization are cost and reliability. In a PEMFC, the major limit on performance is the cathodic oxygen reduction reaction (ORR), multi-electron complex reaction, with slow kinetics both in alkaline and acid media. Also, this cathodic reaction presents a high overpotential and a significant efficiency loss in fuel cell. Pt is the most frequently used catalyst for ORR [1-4]. However, in addition to above considerations, its high cost is also a limiting factor in its use. To avoid these problems, different strategies had been received special attention such as reduce Pt loading [5] or use Pt alloys [6-8], replacement Pt by Pd, Co and Fe [9-12], and Ru based alloys [13-15].

Recently, the research is being direct towards the development of transition-metal nanoparticles supported on carbon, like ruthenium. Se-modified Ru nanoparticles has demonstrated a highly

selective for oxygen reduction to water via four electron pathway (16-17), because its electrochemical properties are modified leading to an increase in its ORR electrocatalytic properties. Nanocrystalline RuM (M = Se, Mo, W, Sn) prepared by mechanical alloying (MA) technique at different milling times showed an increase in specific activities toward the ORR. Evaluation on $Ru_{1-x}Fe_xSe_y$/ catalysts indicated that the ORR activity increases with the increasing of iron and selenium content [14, 18].

In this communication, RuXMo (X=Se,Sn) nanoparticles synthesized by mechanical alloying and supported on Vulcan carbon were evaluated as electrocatalyst for ORR in acid media, searching for an improvement in the electrocatalytic activity through a synergistic effect of Se or Sn and Mo, and enhance of stability of the electrocatalyst. XRD and SEM techniques were used to characterize the catalysts.

2. EXPERIMENTAL

2.1 Preparation of RuXMo electrocatalysts

Preparation of the catalytic powders was achieved by the mechanical alloying (MA) technique of Ru/Se/Mo and Ru/Sn/Mo powders (Aldrich, 99.9 % nominal purity, < 74 μm, < 149 μm, < 10 μm and < 44 μm particle size, respectively), with a ratio of 0.5/0.25/0.25. The powders were introduced in a SPEX 8000 high-energy ball mill using a stainless steel vials and zirconium balls, with a ball to powder ratio of 4:1. The surfactant agent was 1 *wt. %* of isopropanol under inert atmosphere (argon, high purity). Vials were rotated at 1200 rpm for a period of 40 h.

2.2 Materials characterization

X-ray Diffractometer D8 Focus Bruker AXS, equipment with Cu Kα radiation was used for the structure and phase analysis of the MA powders. The XRD patterns were recorded between 20 and 100 ^{0} at a step time of 2 ° min^{-1}. Surface morphology was examined using a scanning electron microscope in a JEOL JSM-6300 operated at 20 kV equipped with an energy dispersive spectrometer.

2.3 Electrochemical measurements

Electrocatalytic evaluation of the powders was carried out by the Rotating Disk Electrode technique (RDE). The working electrode was a vitreous carbon rod electrode (5 mm diameter and cross-sectional area of 0.1963 cm^2) whose surface was previously grinded with 400 and 600 emery papers to adhere the electrocatalyst ink. The ink was prepared mixing 1 mg of each synthesized electrocatalysts with 0.4 mg of Vulcan carbon, 12 μl of Nafion$^®$ and 0.3 ml of ethanol. The mixture was set under ultrasonic treatment to form a homogeneous suspension; 5 μl of suspension were placed by means of a micropipette on the vitreous carbon support, forming a homogeneous thin film. The prepared electrode was dried at room temperature.

The electrochemical measurements were performed in a conventional three-electrode cell (50 ml). A platinum stick was used as counter electrode. The reference electrode was a saturated calomel electrode (SCE) that was inserted separately in a compartment lodging of a Luggin capillary. All potentials were referred to the normal hydrogen electrode (NHE). A 0.5 M H_2SO_4 aqueous solution was used as electrolyte, prepared with deionized water (18.6 MΩcm).

Previously to the electrochemical assessment and surface electrode activation of the working electrode, the acid electrolyte was degassed with high purity nitrogen. Thereafter, the acid electrolyte was saturated with pure oxygen and maintained on the electrolyte surface during the electrochemical experiments. The cell temperature was controlled by a thermostat (PolyScience) at 293 K. The Cyclic Voltammetry (CV) and the Rotating Disk Electrode (RDE) studies were performed with a potenciostat/galvanostat Autolab 30 and an EG&G PAR, model 636 rotation speed controller. The cyclic voltammetry was performed in oxygen free electrolyte from open circuit potential at a $v = 50$ mVs^{-1} for 40 cycles, enough time to reach stable voltammograms. Hydrodynamic experiments were performed in O_2 saturated electrolyte, in the range of rotation rate of 100-1600 rpm at a $v = 5$ mVs^{-1}. The current density values are referred to the geometric electrode surface.

3. RESULTS AND DISCUSSION
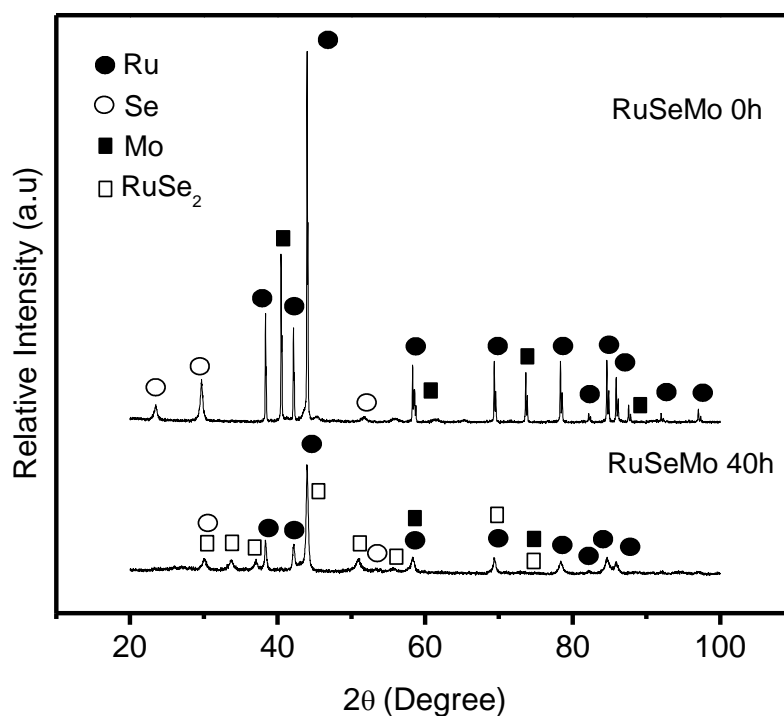
3.1 Physical characterization of the catalysts

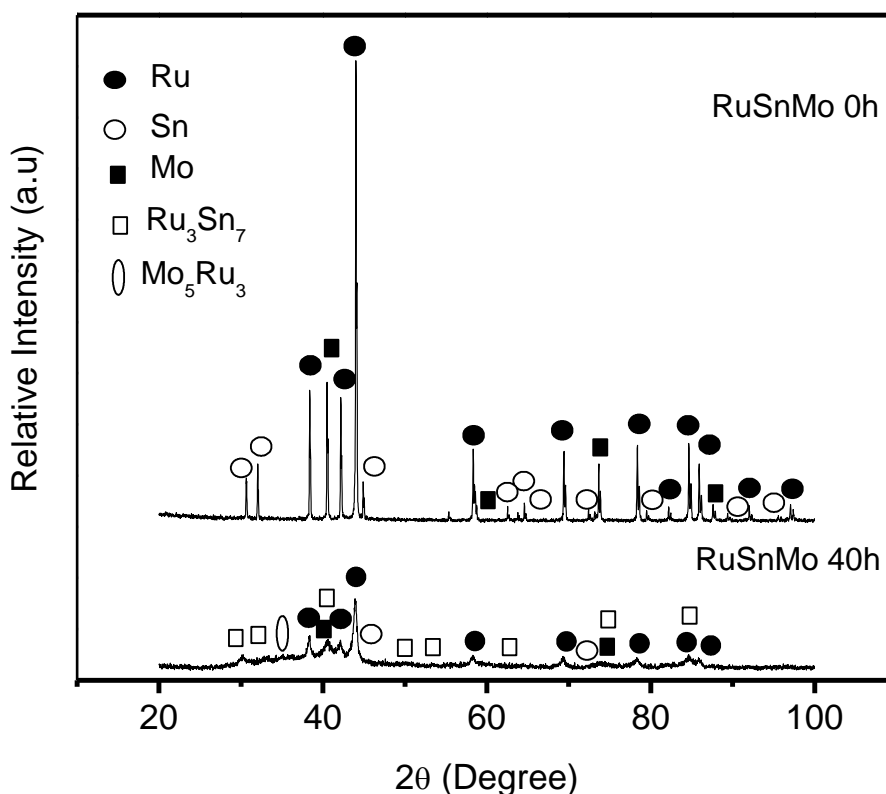**Figure 1.** XRD patterns: RuSeMo at (a) 0 h and (b) 40 h of milling time.

Figure 2. XRD patterns: RuSnMo at (a) 0 h and (b) 40 h of milling time.

X-ray diffraction patterns of RuSeMo and RuSnMo powder mixture at 0 and 40 h of milling are shown in Figure 1 and Figure 2, respectively. It is observed for 0 h of milling in both patterns, a well defined diffraction peaks corresponding to pure phase of each element, except Se peaks that are not well defined because this material has not a metallic character. The X-ray diffraction pattern of RuSeMo to 40 h of milling time shows Ru and Se peaks and the formation of a bimetallic homogeneous phase, $RuSe_2$, this phase was determined by EVA V1.02 software from Bruker. Not observed the formation of any new phase between Mo and the others elements, the Mo peaks are masked with $RuSe_2$ and Ru peaks. This X-ray diffraction pattern shows a broadening and decrease in the intensity of all peaks indicating the reduction of particle size to nanometer order. The calculation to estimate the crystallite size of the dispersed RuSeMo catalyst was based on the broadening of RuM reflection peaks, following the Scherrer´s equation [19].

$$D = \frac{k\lambda}{B\cos\theta} \tag{1}$$

where D is the mean particle size in $\mathring{A}$, k is a coefficient taken here as 0.9, λ the wavelength of the X-rays used (1.540546 $\mathring{A}$), B the width of the diffraction peak at half height in radians, and θ the angle at the position of the maximum peak. From this equation, it was determined that the crystallites size in this system was between 14 and 32 nm. RuSnMo X-ray diffraction pattern to 40 h of milling

time, shows the formation of new phases such as Ru_3Sn_7 and Mo_5Ru_3 indexed by EVA V1.02 software from Bruker. Ru, Sn and Mo peaks are also observed. All peaks are broad and lower intensity indicating the formation of nanometric size crystallites. The crystallite size by Scherrer's equation is between 6 and 15 nm.
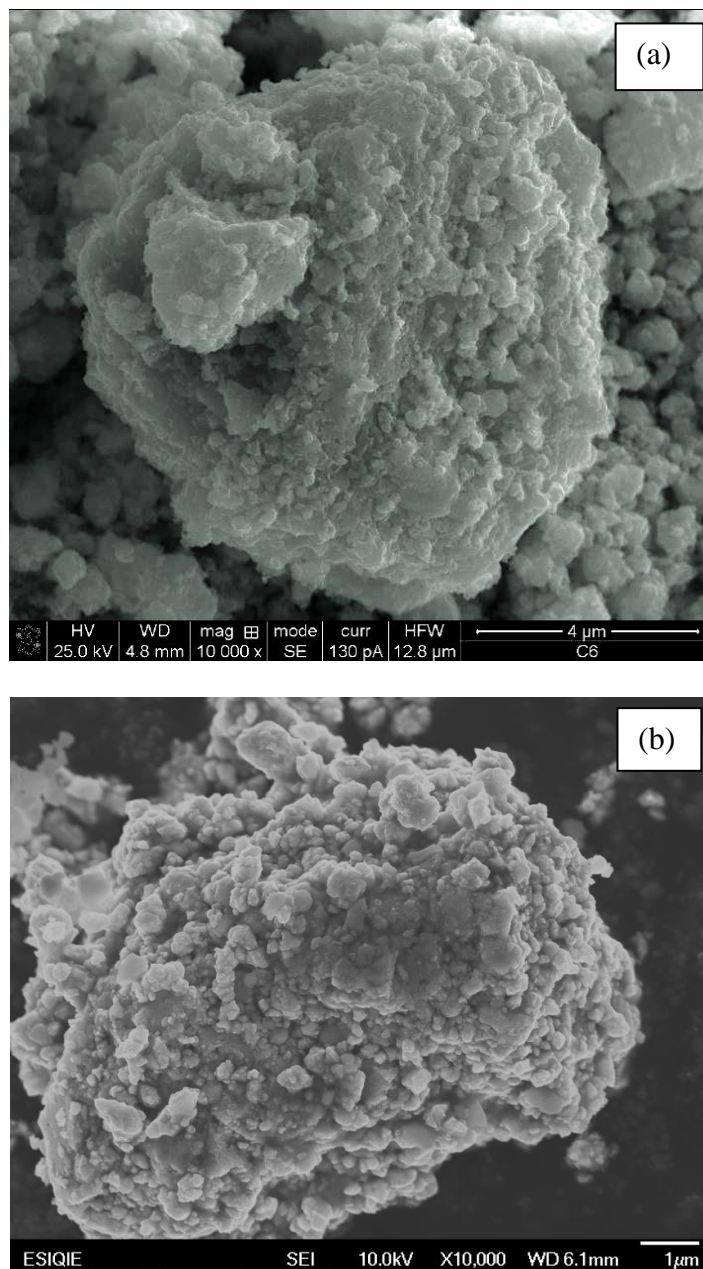

Figure 3. SEM micrographs of synthesized particles a) RuSeMo, b) RuSnMo at 10 000X.

An overall view of electrocatalyst morphology is illustrated by SEM images in Figure 3 (a-b) for RuSeMo and RuSnMo, after 40 h of milling. In these micrographs are observed the components get flattened shapes which have been attributed to a micro-forging process [20]. RuSeMo electrocatalyst presents agglomerated particles between 10-30 μm formed by numerous irregular morphology

particles with sizes between 0.5–3 μm. RuSnMo electrocatalyst shows dispersed particles between 80-400 nm and agglomerated particles between 3-9 μm with irregular morphology.

3.2 Electrochemical evaluation

Initially electrocatalysts were activated by cyclic voltammetry (CV) technique for restructuring the surface at atomic scale, stabilizes the material and increase the activity to ORR [21]. With the activation process was carried out the reduction of the ruthenium oxide surface film. In RuSeMo electrocatalysts, is associated to the formation of mixed oxygen-selenium coverage of the ruthenium particles or to a catalytic influence of selenium on the ruthenium reducibility [22]. In RuSnMo is caused by the overlapping of two stages of the ruthenium surface oxidation Ru(0) to Ru(I) and Ru(II), as suggested by Conway *et.al.*[23].
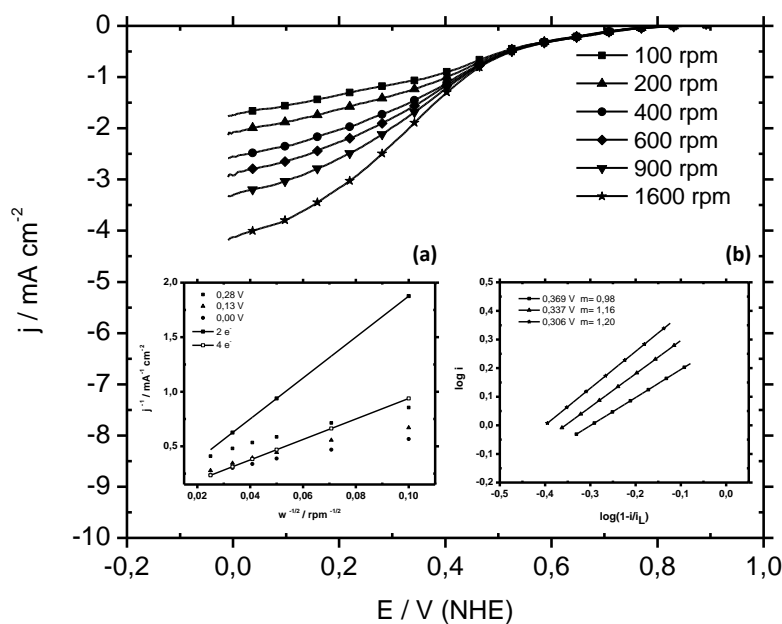

Figure 4. Current potential curves for the molecular oxygen reduction reaction on RuSeMo electrode in O_2 saturated 0.5M H_2SO_4 at 20°C. Inset a) Koutecky Levich plots represented in experimental and theoretical slopes and b) reaction order determination.

Once activated the materials, their electrocatalytic activity for ORR was evaluated by rotating disk electrode technique. Figure 4 shows a set of Rotating Disc Electrode current density-potential curves obtained on RuSeMo electrocatalyst at 25°C, in the range between 0.89 and 0.0085 V/NHE and rotating velocity between 100 and 1600 rpm. It is observed a well defined charge transfer control region in the range of 0.89-0.42 V/NHE, mixed control between 0.42-0.3 V/NHE. However, the mass transport is not well defined. The increment of the rotation rates, increment limiting current due the increase of the oxygen transport to the electrode surface. RuSnMo polarization curves are observed in Figure 5, in the range of 0.76-0.0085 V/NHE. The kinetic control is observed between 0.76-0.48 V/NHE, the mixed control is in the range of 0.48-0.34 V/NHE. RuSnMo polarization curves neither show a well defined diffusional control. In both electrocatalyst do not have a well defined plateau of

the limiting diffusion current, which means that the active sites distribution on these materials is less uniform and the ORR rate is slower. Current density on both materials is the same magnitude order despite the crystallite size obtained by mechanical alloying in the RuSnMo electrocatalyst is approximately 50% lower than RuSeMo, causing particles agglomeration and low material dispersion, also, in the RuSeMo, the particle size distribution is more homogeneous allowing a greater number of active sites in the material surface promoting better electrocatalytic behavior toward the ORR.
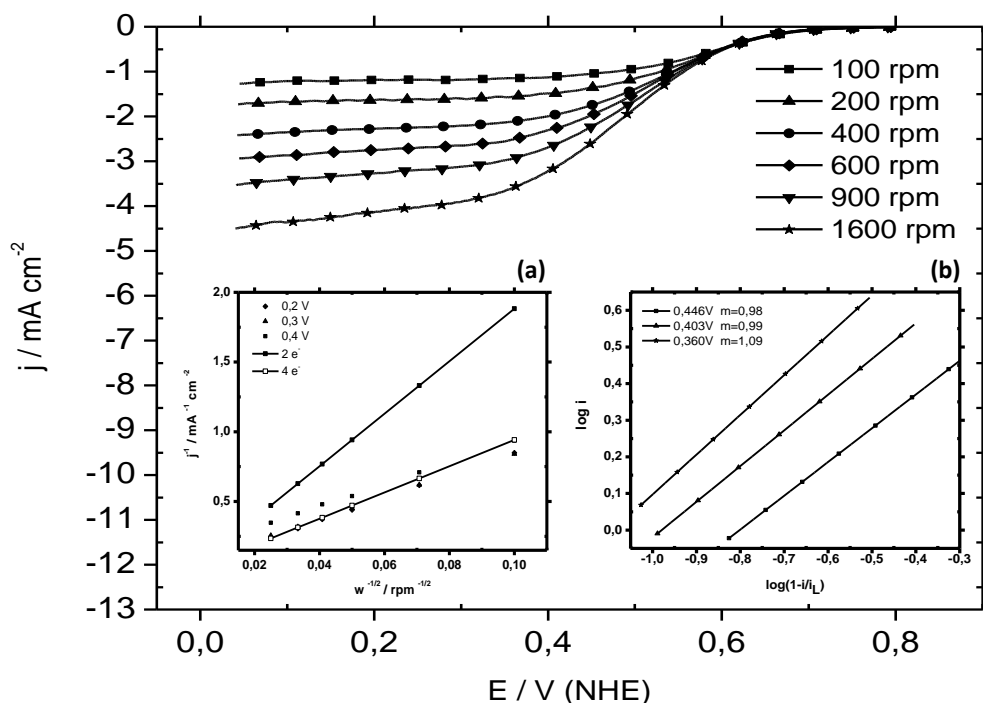

Figure 5. Current potential curves for the molecular oxygen reduction reaction on RuSnMo electrode in O_2 saturated 0.5M H_2SO_4 at 20°C. Inset a) Koutecky Levich plots represented in experimental and theoretical slopes and b) reaction order determination.

Base on the data of RDE measurements from 100 to 1600 rpm, Koutecky Levich (K-L) plots can be expressed with the following equation:

$$\frac{1}{j} = \frac{1}{j_k} + \frac{1}{j_d} = \frac{1}{j_k} + \frac{1}{Bw^{1/2}}$$

(2)

where j_k is the kinetic current density and B is related to the diffusion current density expressed as: $j_d = B\,w^{1/2}$ and w is the electrode rotation rate (rpm). The B parameter is defined as:

$$B = 0.2nFD^{2/3}v^{-1/6}C_{O2}$$

(3)

where B is the Levich slope, 0.2 is a constant used when w is expressed in revolutions per minute, n, the overall electron transfer number, F, the Faraday constant, D, the diffusion coefficient of

oxygen in solution (0.5 M H_2SO_4), v the kinematic viscosity of the H_2SO_4, C_{O2} is the bulk concentration of dissolved oxygen [24]. As proposed by Yeager, the reduction of oxygen in an aqueous solution generally proceeds by either of two pathways [25]. One is a 2e$^-$ pathway to generate the intermediate H_2O_2 with the subsequent decomposition or reduction to generate H_2O, and the other is a 4e- pathway through molecular oxygen is directly reduced to H_2O (ideal reaction). Koutecky Levich plots are illustrated in Figure 4 and 5 (a) for RuSeMo and RuSnMo, respectively. According to the slopes obtained and considering the linearity and parallelism with theoretical slopes to 2e$^-$ and 4e$^-$, the ORR on the electrocatalysts synthesized proceed predominantly by 4e- transfer process indicating the complete reduction of O_2 to water formation, i.e., $O_2 + 4H^+ + 4e^- \rightarrow 2H_2O$. Parallelism of the straight line indicates that the number of electrons transferred per O_2 molecule and the active surface area for the reaction do not change significantly within the potential range studied. The experimental slope (B) of 6.08×10^{-2} mAcm^{-2} for RuSeMo and 7.93×10^{-2} mAcm^{-2} for RuSnMo are in agreement with the theoretical calculated value of 10.63×10^{-2} mAcm^{-2} estimating for ORR of other Ru based compounds [26-28].

The reaction order was evaluated further by plotting log j vs log $((1-j)/j_d)$ using data for polarization curves. The reaction orders are illustrated in Figure 4 and 5 (b). As expected, the slope of the straight lines to RuSeMo and RuSnMo is close to one, confirming a first-order dependence on the kinetics, that corresponds to the transfer of the catalyst first electron to the oxygen adsorbed molecule in the electrode surface, in agreement with the reaction: $(O_2)_{ads} + H^+ + e^- \rightarrow (HO_2)_{ads}$, being the rate determining step of the reduction reaction similar to a Pt catalyst [29].

According to electrode kinetic theory [30], the kinetic current density (j_k) can be expressed as a Tafel form

$$\eta = a - b \, log j_k \tag{4}$$

$$a = \frac{2.3RT}{\alpha F} \log j_o \tag{5}$$

$$b = \frac{2.3RT}{\alpha F} \tag{6}$$

where η, is the overpotential, R, the gas constant, T, the temperature, α, the electron transfer coefficient, F, the Faraday constant, j_o, the exchange current density and b is known as Tafel plot. The Tafel slope can be obtained with the relationship between η and log (j_k) at different potentials. These plots are shown in the Figure 6 and 7 for RuSeMo y RuSnMo, respectively. The Tafel plots show a linear behavior in the mixed activation-difussion region and a deviation of the kinetic current occurs with a higher slope at high current density. The straight line portion observed in the linear region of 0.67-0.58 for RuSeMo and the 0.79-0.73 for RuSnMo was used to determine the kinetic parameters making the current correction for mass transport in the Tafel plots obtained from Figures 6 and 7 and normalized by the active surface area. These regions, known as low field Tafel, show in the inset of Figures 6 and 7.
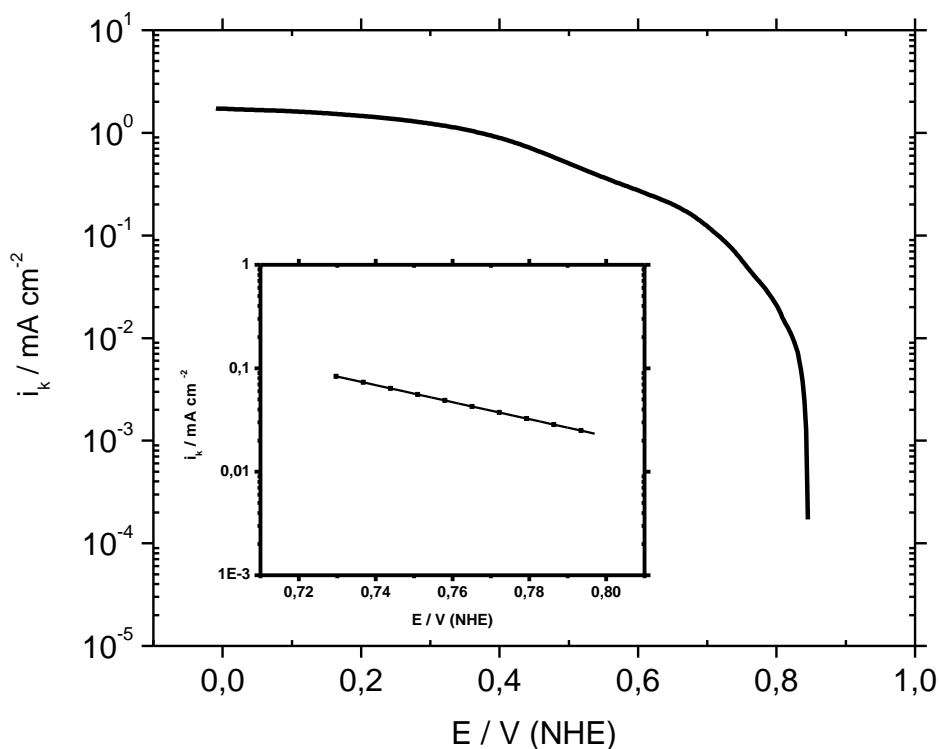
Figure 6. Tafel plots for ORR on RuSeMo electrode in O_2 saturated 0.5M H_2SO_4 at 20°C. Inset: Low field region.
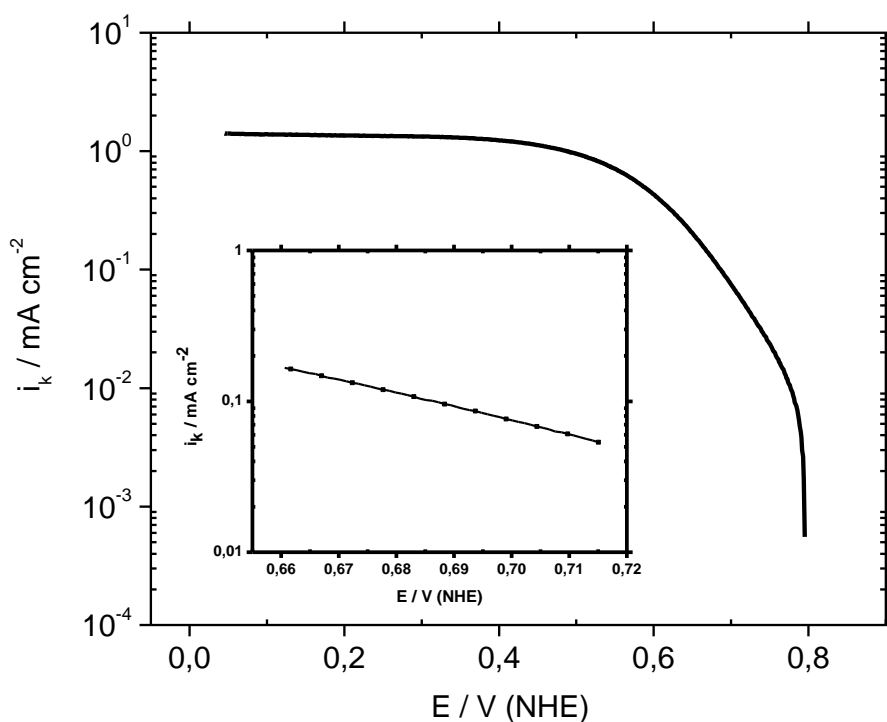

Figure 7. Tafel plots for ORR on RuSnMo electrode in O_2 saturated 0.5M H_2SO_4 at 20°C. Inset: Low field region.
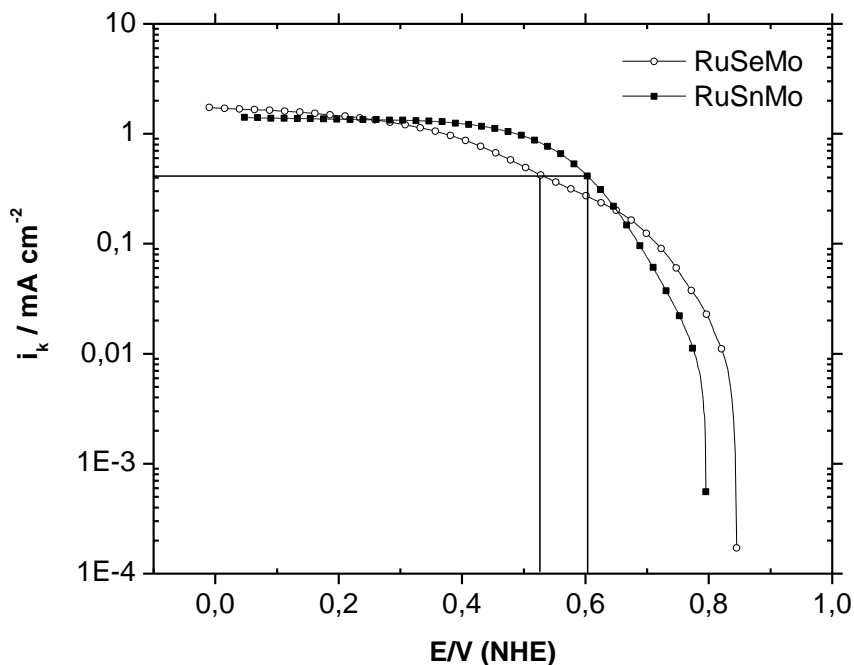
Figure 8. Mass transfer corrected Tafel plots for RuSeMo and RuSnMo corresponding to the potential for attained 0.4 mA cm^{-2}.

Table 1. Kinetic parameters deduced for the oxygen reduction on RuSeMo and RuSnMo electrocatalysts in a 0.5 M H_2SO_4 solution.

Electrocatalyst	$E_1=0$ V/ENH	Reaction Order	- b mVdec^{-1}	α	i_o mA cm^{-2}	N	E V/ENH at i=0.4mAcm^{-2}	η V
RuSeMo	0.811	1.1	121.53	0.487	6.87x10^{-6}	4	0.526	0.418
RuSnMo	0.711	1.04	110.67	0.535	1.31x10^{-6}	4	0.604	0.518

For practical applications, is better to work at a fixed current density and rank the catalysts not in term of exchange current density and mainly in terms of the overpotential, so Figure 8 depicts the corresponding potential attained for 0.4 mA cm^{-2} for RuSeMo and RuSnMo. As one can see, RuSnMo has the overpotential closer to the theoretical potential reversible at this current density and would be considered as the best of both electrocatalyst for ORR in the acid electrolyte al 20 ºC. However, this is not definitive because kinetic current density between 0.28 - 0.65 V / NHE is greater for RuSnMo but at lower potentials less to 0.28 V/NHE and higher than 0.65 V/NHE until the equilibrium potential, the higher current density corresponds to RuSeMo. The kinetics parameters deduced for the ORR on RuSeMo and RuSnMo catalysts at room temperature are presented in Table 1.

Comparing the kinetic parameters of the electrocatalytic materials, the RuSnMo has a better Tafel slope and transfer coefficient, indicating that the potential is better utilized to the activation energy thereby increasing the reaction rate [21]. However, the RuSeMo has better exchange current density meaning that this material is better oxygen adsorber because it has many active sites for ORR

[21] due crystallite size which although not the smallest between the two systems, if an optimal size to be carried out with positive results ORR [18].

Considering the structural and morphological characteristics, RuSnMo presents the best conditions because structurally has smaller crystallites with lower particle agglomeration and more homogeneous morphology.

Electrochemically, both materials present good kinetic characteristics for the ORR. However, taking into account the structural, morphological and electrocatalytic characteristics, the RuSnMo may be considered the best electrocatalytic material for ORR in acid medium in this study. Likewise, this material is economically more convenient for the abundance and low cost of tin.

Electrocatalytic behavior toward ORR of trimetallic catalysts compared to bimetallic catalysts [18], increased due to the synergistic and bifunctional effects modifying the electrical properties of the active centers. In RuSeMo, the Se acts as a electron bridge, faciliting the electronic transfer, besides is a good oxygen adsorber [22,31-33]. In RuSnMo, the Ru and Sn are oxophilic and promote the oxygen donation and reduces the overpotential of ORR [34] besides the Mo facilitates the electron delocalization, causing a high conductivity [35] in both electrocatalysts.

4. CONCLUSIONS

The present study demonstrates that mechanical alloying is an effective method for the preparation of nanometric RuSeM and RuSnMo electrocatalysts. The physical characterization of RuSeMo showed the formation of a bimetallic homogeneous phase, $RuSe_2$, and Ru and Se free with irregular morphology and crystallite size between 14-32 nm; for RuSnMo, the formation of two intermetallic compounds, Ru_3Sn_7 and Mo_5Ru_3, and Ru, Sn and Mo free with crystallite size between 6-15 nm and irregular morphology. The kinetic experiments indicated that the trimetallic electrocatalysts improved the catalytic activity selectivity toward the four electron reduction of molecular oxygen to water formation. The electrocatalytic activity and stability of these trimetallic catalysts increased compared with bimetallic catalysts of the same elements by synergistic, bifunctional and electronics effects.

References

1. H.A. Gasteiger, S.S. Kocha, B. Sompalli, F.T. Wagner, *Appl. Catal.* B, 56 (2005) 9.
2. A. Bonakdarpour, K. Stevens, G.D. Vernstrom, R.T. Atanasoski, A.K. Schmoeckel, M.K. Debe, J.R. Dahn, *Electrochim. Acta,* 53 (2007) 688.
3. X. Yu, S. Ye, J. *Power Sources,* 172 (2007) 133.
4. E. Antolini, *Mater. Chem. Phys,* 78 (2003) 563.

5. J.H. Wee, K.Y. Lee, S.H. Kim, *J. Power Sources,* 165 (2007) 667.
6. A. Seo, J. Lee, K. Han, H. Kim, *Electrochim. Acta,* 52 (2006) 1603.
7. M. Lischka, C.Mosch, A. Grob, *Electrochim. Acta,* 52 (2007) 2219.
8. F.H.B. Lima, W.H. Lizcano, E. Teixeira F.C. Nart, E.R. González, E.A. Ticianelli, *Electrochim. Acta,* 52 (2006) 385.
9. S. Thanasilp, M. Hunsom, *Renewable Energy,* 36 (2011) 1795.
10. Y. Tamura, K. Taneda, M. Ueda, T. Ohtsuka, *Corros. Sci.,* 51 (2009) 1560.
11. T. Toda, H. Igarashi, M. Watanabe, *J. Electroanal. Chem.,* 460 (2011) 258.
12. M. Neergat, V. Gunasekar, R. Rahul, *J. Electroanal. Chem.,* 658 (2011) 1.
13. A. Lewera, J. Inukai, W.P. Zhou, D. Cao, H.T. Duong, N. Alonso-Vante, A. Wieckowski, *Electrochim. Acta,* 52 (2007) 5759.
14. A. Ezeta, E.M. Arce, O. Solorza, R.G. González, H. Dorantes, *J. Alloys Compd.,* 483 (2009) 429.
15. C. Delacôte, A. Lewera, M. Pisarek, P. J. Kulesza, P. Zelenay, N. Alonso Vante, *Electrochim. Acta,* 55 (2010) 7575.
16. C.M. Johnston, D. Cao, J.H. Choi, P.K. Babu, F. Garzon, P. Zelenay, *J. Electroanal. Chem,* 662 (2011) 257.
17. K. Suárez, A. Rodríguez, S. Durón, O. Solorza, *J. Power Source,* 171 (2007) 381.
18. A. Ezeta, O. Soloza, H.J. Dorantes, J.M. Hallen, E.M. Arce, *Int. J. Electrochem. Sci*., 7 (2012) 8940.
19. B.D. Cullity, *Elements of X-Ray Diffraction*, Addison-Wesley Publishing Company, INC., USA (1978).
20. M.R. Paruchuri, D.L. Zhang, T.B. Massalski, *Mater. Sci. Eng.* A, 174 (1994) 119.
21. P. Sotelo, R.G. González, J.G. Cabañas, O. Solorza, *Int. J. Electrochem. Sci.,* 2 (2007) 523.
22. M.Bron, P. Bogdanoff, S. Fiechter, I. Dorbandt, M. Hilgendorff, H. Schulenburg, H. Tributsch, *J. Electroanal. Chem.,* 500 (2001) 510.
23. S. Hadzi Jordanov, H. Angerstein Kozlowska, M. Vuckovic, B.E. Conway, *J. Phys. Chem.,* 81 (1977) 2271.
24. N.A. Anastasijevic, V. Vesovic, R.R. Adzic, *J. Electroanal. Chem.,* 229 (1987) 305.
25. Y. Otake, R.G. Jenkins, *Carbon*, 31(1) (1993) 109.
26. R.G. González, R. González, S. Citalán, C. Montero, O. Solorza, *J. New Mater Electrochem Syst.,* 8 (2005) 15.
27. R. González, O. Solorza, *J. Solid State Electrochem.,* 7 (2003) 289.
28. T.J. Schmidt, U.A. Paulus, H. Gasteiger, N. Alonso Vante, R.J. Behm, *J. Electrochem. Soc*., 147 (2000) 2620.
29. O. Solorza. O, Ellmer K, Giersig M, Alonso-Vante N, *Electrochim Acta,* 39 (1994) 1647.
30. Bard AJ, Faulkner LR. *Electrochemical methods: Fundamentals and applications,* 2nd Ed. New York: John Willey & Sons (2001).
31. H. Cheng, W. Yuan, K. Scott, *Electrochim. Acta,* 52 (2006) 466.
32. K.S. Nagabhushana, E. Dinjus, H. Bönnemann, V. Zaikovskii, C. Hartnig, G. Ehl, I. Dorbandt, S. Fiechter, P. Bogdanoff, *J. Appl. Electrochem*., 37 (2007) 515.
33. M. Montiel, S. García Rodríguez, P. Hernández Fernández, R. Díaz, S. Rojas, J.L. Fierro, E. Fatás, P. Ocón, *J. Power Sources,* 195 (2010) 2478.
34. M.T.M. Koper, *Surface Science,* 548 (2004) 1.
35. N. Alonso Vante, W. Jaegermann, H. Tributsch, W. Honle, K. Yvon, *J. Am. Chem. Soc.,* 109 (1987) 3251.